

Isotope-Purification-Induced Reduction of Spin-Relaxation and Spin-Coherence Times in Semiconductors


Oscar Balancea-Lindvall¹,¹ Matthew T. Eiles²,² Nguyen Tien Son¹,¹ Igor A. Abrikosov¹,¹ and Viktor Ivády^{1,2,3,4,*}

¹Department of Physics, Chemistry and Biology, Linköping University, Linköping SE-581 83, Sweden

²Max-Planck-Institut für Physik komplexer Systeme, Nöthnitzer Street 38, Dresden D-01187, Germany

³Department of Physics of Complex Systems, Eötvös Loránd University, Egyetem tér 1-3, Budapest H-1053, Hungary

⁴MTA–ELTE Lendület “Momentum” NewQubit Research Group, Pázmány Péter, Sétány 1/A, Budapest 1117, Hungary

 (Received 20 May 2022; revised 15 March 2023; accepted 18 May 2023; published 15 June 2023)

Paramagnetic defects and nuclear spins are often the major sources of decoherence and spin relaxation in solid-state qubits realized by optically addressable point defect spins in semiconductors. It is commonly accepted that a high degree of depletion of nuclear spins can enhance the coherence time by reducing magnetic noise. Here we show that the isotope purification beyond a certain optimal level can become counterproductive when both electron and nuclear spins are present in the vicinity of the qubits, particularly for half-spin systems. Using state-of-the-art numerical tools and considering the silicon-vacancy qubit in various spin environments, we demonstrate that the coupling of the spin-3/2 qubit to a spin bath of spin-1/2 point defects in the lattice can be significantly enhanced by isotope purification. The enhanced coupling shortens the spin-relaxation time that in turn may limit the coherence time of spin qubits. Our results can be generalized to triplet point defect qubits, such as the nitrogen-vacancy center in diamond and the divacancy in silicon carbide.

DOI: [10.1103/PhysRevApplied.19.064046](https://doi.org/10.1103/PhysRevApplied.19.064046)

I. INTRODUCTION

Point defect qubits in semiconductors exhibit long coherence time at cryogenic and room temperature [1–3]. Combining this feature with advanced magneto-optical control of the qubit state has enabled these systems to become the leading contender in several areas of quantum technology [4–6]. The properties of point defect qubits depend to a very large degree on the host material. In particular, magnetic fluctuations in the local spin environment of the defects can profoundly influence the defect’s coherence time, in most cases reducing it by several orders of magnitude from the theoretical upper limit set by the spin-relaxation time [1,7]. As a result, a strategy of chemical and isotope purification in the host material is commonly pursued in order to enhance the coherence time of the point

defect qubits. It is believed that this strategy can be applied in most of the cases [1,7–12].

In this paper, we report on a counterintuitive effect that emerges when both electron and nuclear spins are present in the vicinity of the qubits. In particular, we show that isotope purification leads to a significant reduction of the spin-relaxation time, due to enhanced cross-relaxation effects with other paramagnetic defects of similar fine structure. This effect in turn sets a reduced upper limit for the coherence time. We study the phenomenon numerically for the quartet silicon-vacancy center (V_{Si}) in silicon carbide (SiC), where the consequences may be highly significant. Our results can be extended to other semiconductor quantum systems, such as quantum dot spin qubits in silicon.

The negatively charged silicon vacancy in SiC exhibits a quartet ground-state spin with long coherence time [3,13]. This high spin state has been utilized in quantum sensing applications [14–21] and to implement a room-temperature maser [22]. Furthermore, the defect’s favorable optical properties [23,24] and advanced fabrication capabilities [25–27] make it potentially interesting for near-infrared quantum information processing applications [22,26–32]. In 4H-SiC, the V1 and V2 photoluminescence lines and the Tv1-Tv2 electron spin resonance

* viktor.ivady@liu.se

Published by the American Physical Society under the terms of the [Creative Commons Attribution 4.0 International](https://creativecommons.org/licenses/by/4.0/) license. Further distribution of this work must maintain attribution to the author(s) and the published article’s title, journal citation, and DOI. Funded by [Bibsam](https://www.bibsam.com/).

(ESR) signals [33–37] are related to the negatively charged silicon vacancy. The V1 and V2 center are assigned to the h and k silicon-vacancy configurations, respectively, by comparing with first-principles results [38,39]. In our numerical studies we consider the V2 center, which is the most often studied configuration.

There are two main ingredients of the environmental spin bath in SiC. Natural samples include 4.7% ^{29}Si and 1.1% ^{13}C spin-1/2 nuclear spins. In addition, the structure of the host material incorporates various paramagnetic defects and impurities, whose concentrations may vary over several orders of magnitudes depending on the growth conditions, after growth sample preparation, and nanoscale fabrication. Here, we consider the most common intrinsic spin-1/2 defects, such as the carbon vacancy and carbon-antisite-vacancy pair whose concentration can reach 10^{15} cm^{-3} in HPSI 4H-SiC [30,40]. We note that this value may increase by 2–3 orders of magnitude due to irradiation and implantation that are frequently used techniques to create silicon-vacancy qubits.

II. METHODS

In our study, we divide the complex ground-state spin Hamiltonian of the quartet silicon-vacancy-environmental spin-bath system into two terms, H_1 and H_2 , respectively, describing one- and two-spin interaction terms. The one-spin interactions include the zero-field splitting (ZFS) interaction of the quartet silicon vacancy and Zeeman terms of all the spins in the system, i.e.,

$$H_1 = D \left(S_{0,z}^2 - \frac{5}{4} \right) + g_{3\parallel} \mu_B \frac{S_{0,+}^3 - S_{0,-}^3}{4i} B_z + g_e \mu_B \sum_{j=0}^N S_{j,z} B_z + \mu_N \sum_{k=1}^M g_{N,k} I_{k,z} B_z, \quad (1)$$

where $S_{j,z}$ is the z component of the electron spin operator of defect j , $I_{k,z}$ is the z component of the nuclear spin operator of nucleus k , g_e is the electron g factor, μ_B is the Bohr magneton, $g_{N,k}$ is the nuclear g factor of nucleus k , and μ_N is the nuclear magneton. Terms with $j = 0$ index label the silicon-vacancy spin, while $j > 0$ indices label the doublet paramagnetic defects in the environment. The ZFS parameter D is equal to 35.0 MHz for the V2 silicon-vacancy configuration [38]. The second term on the rhs of Eq. (1) accounts for a nonvanishing higher-order term of the Zeeman interaction of the quartet spin states in C_{3v} symmetry, where $g_{3\parallel} = 0.6$ [16,41].

The two-spin interaction terms account for the hyperfine and the dipolar coupling between qubit and spin-1/2 electron spins, as well as dipolar coupling between nuclear

spins, i.e.,

$$H_2 = \sum_{j=0}^N \sum_{k=1}^M \mathbf{S}_j A_{jk} \mathbf{I}_k + \sum_{i=0}^N \sum_{j>i}^N \frac{\mu_0 g_e^2 \mu_B^2}{4\pi r_{ij}^3} (\mathbf{S}_i \mathbf{S}_j - 3 (\mathbf{S}_i \hat{\mathbf{r}}_{ij}) (\mathbf{S}_j \hat{\mathbf{r}}_{ij})) + \sum_{k=1}^M \sum_{l>k}^M \frac{\mu_0 g_{N,k} g_{N,l} \mu_N^2}{4\pi r_{kl}^3} (\mathbf{I}_k \mathbf{I}_l - 3 (\mathbf{I}_k \hat{\mathbf{r}}_{kl}) (\mathbf{I}_l \hat{\mathbf{r}}_{kl})), \quad (2)$$

where A_{jk} is the hyperfine tensor, $\hat{\mathbf{r}}_{ij}$ and r_{ij} are the unit vector and distance between spin i and spin j . A_{jk} for $j > 0$ are mostly unknown as they depend on the paramagnetic defects found in the vicinity of the silicon vacancy. For simplicity, we consider only the hyperfine interaction of the silicon vacancy, i.e., $A_{jk} = 0$ for $j > 0$, and use the hyperfine coupling tensors obtained from first-principles density-functional-theory calculations in Ref. [42]. However, beyond 15 Å distance from the silicon vacancy, the Fermi contact term is neglected and only the dipolar hyperfine term is considered. All presented couplings are temperature-independent contributions to the spin interactions in the lattice and our numerical models do not include temperature-dependent spin-lattice relaxation effects.

In order to numerically study the Hahn-echo coherence time (T_2) of the quartet silicon-vacancy spin in natural and isotope purified SiC, we employ the second-order generalized cluster-correlation expansion (gCCE-2) method [43]. In contrast to popular collective field models, which assume a statistical model of the spin-bath fluctuations frequently requiring experimental parameters [44,45], the gCCE-2 approach, as well other approaches in this work, allow simulation based on a microscopic model obtainable via first-principles techniques. An outline of the method is provided in Appendix A.

The numerically converged models include $M \approx 1000$ nuclear spins within a sphere of radius r_{bath} around the qubit. For natural nuclear spin abundance models $r_{\text{bath}} = 50$ Å is used, while for lower abundances r_{bath} is increased to keep the average number of environmental spins M fixed. Nuclear spin pairs are considered within the cut-off radius $r_{\text{dip}} = 6.0$ Å. The ensemble coherence function is obtained by averaging over 500 randomly generated spin-bath configurations and fitted with an $A \exp(-t/T_2^n)$ function to obtain the Hahn-echo coherence time T_2 . To study the coherence properties of the silicon vacancy, the $|+3/2\rangle$ and the $|+1/2\rangle$ states are used to implement a qubit.

In order to quantify the dipolar spin-relaxation time (T_1) of the quartet silicon-vacancy spin states in a bath of spin-1/2 electron spins, we utilize the method recently developed in Ref. [42] and briefly reviewed in Ref. [46].

This approach utilizes a clustering scheme to reduce the complexity of the spin population evolution under the assumption of weak intrabath interactions. In this regime, the interaction between bath spins may be neglected in favor of reducing the Hilbert space of the problem while still approximating the evolution of the N -body defect and bath system. For details, see Appendix B.

The considered spin-bath models include $N = 32$ electron spins with varying concentration, forming a closed system with the defect. We use the first-order cluster approximation, constraining the Hamiltonian coupling terms to that of pairwise defect-bath interactions, which is suitable for an electron spin bath of short coherence time [42,46]. The time step of the propagation is set to 1 ps, while the simulation time is optimized for the considered concentrations and vary between 0.05 and 1 ms.

Local inhomogeneities at the defect sites due to the hyperfine interaction are included in calculations as an effective magnetic field. Accordingly, the first term on the rhs of Eq. (2) is approximated as $H_{\text{inhomo}} = \Delta S_{0,z}$, where $\Delta = \sum_k A_{0k,z} \langle I_{k,z} \rangle$ is the inhomogeneous splitting, or the nuclear Overhauser field in other contexts. Here, the angular bracket represents expectation value, while $A_z = \sqrt{A_{xz}^2 + A_{yz}^2 + A_{zz}^2}$. The coupling strength between the qubit and the bath spins are obtained in the point-spin density approximation, i.e., by assuming spin dipole-dipole interactions. The $S_{0,+}S'_{j,-} + S_{0,-}S'_{j,+}$ term contained within the second term in the rhs of Eq. (2) can effectively couple the quartet and doublet states of the defect-bath spin cluster.

III. RESULTS

First, we study the coherence time of the V2 silicon-vacancy qubit when *only nuclear spins* are included in the spin bath. The decay of the Hahn-echo coherence function due to a surrounding nuclear spin bath of natural isotope abundance is depicted in Fig. 1. As can be seen, the coherence function decays on two different time scales. Due to the hyperfine interaction driven precession of the nuclear spins, the coherence function partially collapses at first with a time scale comparable with the inhomogeneous coherence time (T_2^*). In contrast to the N-V center, the coherence function does not recover later and no coherent beatings can be observed. This irregular behavior is due to the quartet spin state and further discussed in Ref. [47]. The long time scale decay, observable in Fig. 1, is due to the nuclear spin-nuclear spin interaction induced magnetic field fluctuations. The former effect dominates at small magnetic field values, i.e., at strong hyperfine coupling, while the latter effect dominates at high magnetic field values where the hyperfine interaction is suppressed by the Zeeman splitting of the nuclear spin states. The coherence time saturates above $B = 200$ Gauss and takes the values of $T_2 = 1.8$ ms for natural abundance of paramagnetic nuclei. The strength of the nuclear-spin coupling and

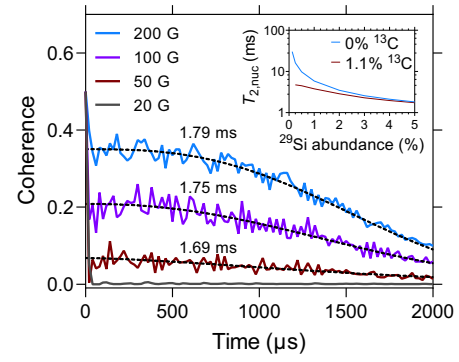


FIG. 1. Coherence of the quartet V2 center in a nuclear spin bath in 4H-SiC. Decay of the coherence function at various magnetic field values for natural abundance of nuclear spins. The coherence time is provided for each curve. For $B > 200$ G the coherence time saturates and takes the value of $T_2 = 1.8$ ms. The inset shows ^{29}Si abundance dependence of the saturated coherence time at $B = 200$ G.

thus the saturated high magnetic field coherence time sensitively depend on the abundance of the nuclear spins. As expected, the T_2 time significantly enhances as the nuclear-spin bath is depleted, see inset of Fig. 1. These results are in accordance with the anticipated behavior of the system and previous results on the coherence time of the silicon vacancy [47].

However, the host material includes not only nuclear spins but also other *electron-spin defects* in the local environment of the qubits. In order to qualitatively understand the behavior of a quartet electron spin interacting with a bath of spin-1/2 defects, let us first consider the magnetic field dependence of the energy levels of a *single quartet-doublet electron-spin pair* in Fig. 2(a), as opposed to the many-spin system considered in our quantitative simulations. The relevant physics of the many-spin system can be understood by considering such a 2-spin subsystem. As can be seen in Fig. 2(a), for large magnetic field values the Zeeman interaction dominates. Due to the magnetic splitting of both the quartet and the doublet electron spins ($g_e \approx 2$ for both spins), the energy levels form five distinct branches, labeled in Fig. 2(a). Note that each of the three innermost branches consist of a pair of states. These pairs include $\Delta m_S = \pm 1$ and $\Delta m_{S'} = \mp 1$ states of the quartet and the doublet states and can be effectively coupled by the dipole-dipole interaction. This interaction induces spin flip flops of the electron spins, shortens the spin-state lifetime, and thus limits the coherence time of the quartet silicon-vacancy qubit states.

Since the dipolar coupling of the electron spins is generally small, any splitting of the spin states within the branches has a significant effect on the lifetime of the states. In this respect, it is noteworthy that the $|+1/2, -1/2\rangle$ and the $|-1/2, +1/2\rangle$ states are degenerate, when only ZFS and Zeeman interactions are taken into

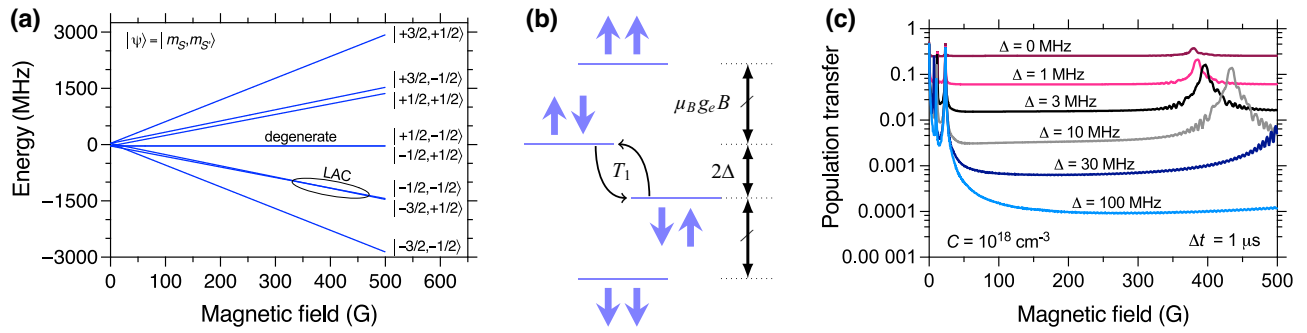


FIG. 2. Resonant coupling of a quartet electron spin and doublet electron spins. (a) Energy levels of a *single* quartet-doublet two-electron spin system, meant to provide qualitative intuition of the otherwise complex many-body system under consideration. The corresponding states are provided in the $|m_S, m_S'\rangle$ basis, where the quantization axes is set parallel to the c axis. (b) Illustration of the spin energy levels of the $m_S = \{\mp 1/2, \pm 1/2\}$ subspace of the quartet-doublet electron-spin pair upon hyperfine splitting Δ , affecting the sensitive spin-flip frequency between the usually nearly degenerate states. (c) Thermalization of the quartet spin states in a bath of spin-1/2 electron spins, for various inhomogeneous splittings Δ of the silicon-vacancy states. The vertical axis measures the amount of population transferred from the initial highly polarized $m_S = +1/2$ state to the rest of the quartet states of the V2 center under a fixed evolution time of $\Delta t = 1 \mu\text{s}$ in a bath of spin-1/2 electron spin of $C = 10^{18} \text{ cm}^{-3}$ concentration.

consideration, see Fig. 2(a). These states have a fundamental role for the silicon-vacancy qubit, as the $|+3/2\rangle \leftrightarrow |-3/2\rangle$ transition is not directly addressable via microwave irradiation. In contrast, the zero-field interaction splits the states in other branches. Due to the higher-order terms of the Zeeman interaction of the quartet silicon vacancy, the states within a branch may cross each other, see, for instance, the region labeled by LAC in Fig. 2(a).

In order to study the thermalization of the silicon-vacancy spin states in an electron-spin bath, we simulate the population transfer from the initially highly polarized $|+1/2\rangle$ state to the rest of the quartet spin states in our many-spin model, see Fig. 2(c). When the $|+1/2, -1/2\rangle$ and $| -1/2, +1/2\rangle$ states are degenerate, the initial population thermalizes within $1 \mu\text{s}$ irrespective of the external magnetic field, see the uppermost curve in Fig. 2(c). On the other hand, by introducing an effective inhomogeneous magnetic field acting on the quartet spin state and causing a Δ splitting in the $m_S = \{-1/2, +1/2\}$ subspace of the quartet spin, as illustrated in Fig. 2(b), the magnetic-field-independent component of the spin relaxation reduces drastically, indicating the elongation of the spin-state lifetime at most magnetic field values. The remaining high population transfer peaks, below 50 G and at around 400–500 G in Fig. 2(c), are related to level anticrossings (LACs) of the spin states that are studied in more details in Ref. [48]. Furthermore, we note that the reduced lifetime of the $m_S = \{-1/2, +1/2\}$ state, beyond the theoretical expectations [19], has been recently reported in Ref. [49] and has been attributed to the coupling to spin-1/2 defects. These results indicate that the inhomogeneous splitting of the spin states plays a crucial role in elongating the spin-state lifetime in an electron-spin bath.

There are several different sources of local inhomogeneous fields that, in principle, could induce a splitting of

the degenerate subspace of the coupled quartet-doublet spin states and suppress the mutual flip flops of the spins. Strain and electric fields may impact the energy levels of defect spins. However, half-spin systems remain degenerate under the influence of such fields according to Kramer’s theorem. One may also consider an effective Landé g factor deviating from the electron factor g_e , e.g., a vanadium defect in $4H\text{-SiC}$ with $g \approx 1.95$ [50], which would introduce a permanent splitting of the $m_S = \{\mp 1/2, \pm 1/2\}$ subspace. However, such a splitting would be magnetic field dependent and considerable mainly in the regime dominated by the Zeeman splitting term. In most cases, hyperfine coupling is typically the strongest interaction that can give rise to local inhomogeneities on subnanometer scales.

In order to quantify the hyperfine interaction-induced inhomogeneity, we study the distribution of the hyperfine splitting of the $m_S = \{-1/2, +1/2\}$ subspace of the quartet silicon vacancy, Δ , shown in Fig. 3. The distribution exhibits several distinct and isolated peaks. The largest peak corresponds to configurations with no first and second nearest-neighbor nuclear spins. Going from lower to higher splitting, the second, third, and fourth peaks include configurations with one, two, and three second nearest-neighbor ^{29}Si nuclear spins. This series continues with vanishing peak heights. Furthermore, there are two additional noticeable peaks beyond 20 MHz that correspond to one ^{13}C and zero ^{29}Si nuclear spin and one ^{13}C and one ^{29}Si nuclear spins in the first and second neighborhood shell of the silicon vacancy.

The hyperfine interaction-induced local inhomogeneity is approximated by an inhomogeneous magnetic field acting on the silicon vacancy, which splits the $m_S = \{-1/2, +1/2\}$. The field is here defined as the median of the effective hyperfine strength

distribution of the random environment ensemble, i.e., as median $\left(\sum_k \sqrt{A_{k,xz}^2 + A_{k,yz}^2 + A_{k,zz}^2}\right)$ for hyperfine tensor components between the qubit and nuclear spins, k denoting the nuclear-spin index within each spin configuration. We note that a single value cannot properly characterize a multipeak distribution observed in Fig. 3, however, in paramagnetic isotope depleted samples the amplitude of the peaks beyond the first peak are significantly reduced and the distribution converges to a single peak-asymmetric distribution. In such cases, the median is a good measure of the distribution of the maximal hyperfine splitting. The median as a function of the ^{29}Si abundance is depicted in the inset of Fig. 3. As can be seen, the median of the hyperfine splitting approaches zero as the paramagnetic silicon isotopes are depleted.

Combining our results presented so far, we conclude that the isotope purification can reduce the inhomogeneous splitting of the qubit states, which in turn may enhance the coupling and cross-relaxation effects between the quartet spin states and spin-1/2 defects in the local environment, see Fig. 2(c). This counterintuitive phenomena may lead to a drastically reduced spin-state lifetime that sets the maximum for the coherence time. To quantify this effect, we calculate the spin relaxation time T_1 of the $|+1/2\rangle$ state of the silicon vacancy for various spin-1/2 paramagnetic point defect concentrations, as a function of the ^{29}Si abundance and zero ^{13}C abundance. The choice of ^{13}C abundance simplifies the analysis and may be justified by the fact that ^{29}Si and ^{13}C relaxation and decoherence contributions are comparable mainly at similar abundances (e.g., see inset of Fig. 1). At the same abundances, ^{13}C may yield a stronger splitting field due to its larger nuclear magnetic moment

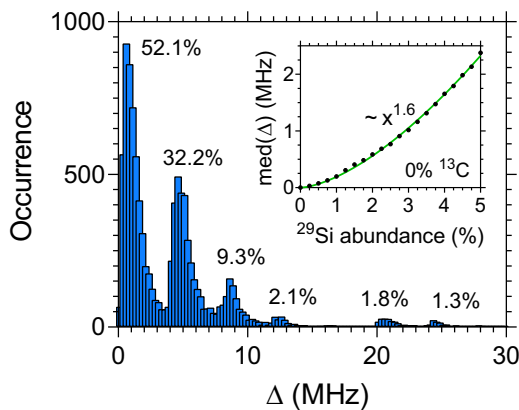


FIG. 3. The distribution of the hyperfine splitting Δ of the $m_S = \{-1/2, +1/2\}$ subspace of the quartet electron spin in natural abundance. The inset shows the variation of the median of the hyperfine splitting distribution, including calculated medians and a power-law fit, as a function of the paramagnetic ^{29}Si abundance, with no carbon isotope spins.

and first neighbor proximity. However, we do not expect any qualitative differences for different nuclear-spin types.

We define the absolute maximum of the coherence time as $T_{2,\text{max}} = 2T_1$. Here, we note that in experiments $T_{2,\text{max}} \approx 0.5T_1$ is found for the N-V center [9], therefore our results can be considered as an upper bound. To obtain the coherence time when both nuclear spins and electron spins are included in the local environment of the silicon vacancy, we use the $T_2^{-1} = T_{2,\text{max}}^{-1} + T_{2,\text{nuc}}^{-1}$ relation, where the last term accounts for decoherence effects due to nuclear-spin flip-flop-induced magnetic fluctuations.

The results on the ensemble averaged coherence time are depicted in Fig. 4. The individual relaxation times and coherence times are shown in Appendix C. As can be seen the coherence time can be significantly reduced both by the increase of the electron-spin concentration and the depletion of the paramagnetic isotopes. In high spin-1/2 defect concentration (approximately equal to 10^{18} cm^{-3}) T_2 is limited by the paramagnetic defects and cannot reach higher than approximately 100 μs . As the defect concentration reduces, the theoretical maximum of the coherence time rapidly increases and the fluctuation of the nuclear-spin bath starts to limit the coherence time in natural abundance, see the calculated T_2 time at, for instance, natural abundance of ^{29}Si isotope in Fig. 4. Isotope purification not only reduces magnetic field fluctuations but also enhances cross-relaxation effects that may become the major limiting factor in the coherence time in nuclear-spin depleted samples, see Fig. 4. We note that even a very low concentration of spin-1/2 defect may have a dramatic effect on the coherence time in highly isotope purified samples.

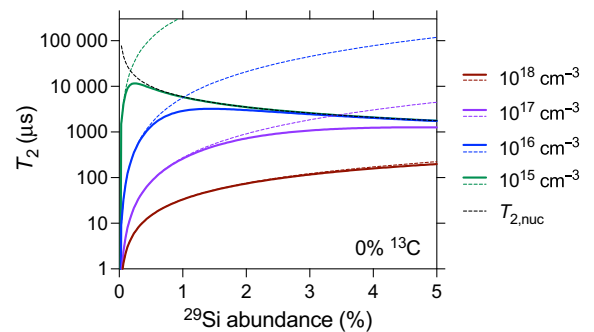


FIG. 4. Paramagnetic ^{29}Si abundance dependence of the spin-coherence time at various spin-1/2 point defect concentrations. $T_{2,\text{nuc}}$ (dashed black line) is obtained at 200 G by including ^{29}Si nuclear spins in the environment only. The theoretical maximum of the coherence time $T_{2,\text{max}}$ is set by spin relaxation due to electron spins (plotted by colored dashed lines). The coherence time T_2 is obtained by combining these effects (colored thick solid lines).

IV. DISCUSSION AND CONCLUSION

Temperature-dependent relaxation effects and other magnetic-field-independent effects are not accounted for in Fig. 4 and may become relevant for less purified samples. These contributions will provide an additional term to the relaxation rate, setting an upper bound on the T_1 time. Photoluminescence and electron paramagnetic resonance measurements have estimated the relaxation time of the silicon vacancy in a sample of natural abundance at room temperature to approximately 40–100 μs [51,52], setting the upper bound on $T_{2,\text{max}} = 2T_1$ below the limit of a 10^{17} cm^{-3} electron-spin-bath concentration up to natural ^{29}Si abundance. Measurements at lower temperatures showed a roughly exponentially decreasing trend of the relaxation rate, with T_1 times of 400 μs at 200 K and 1700 μs at 100 K [52]. Therefore, the enhanced hyperfine-driven relaxation studied in this work, limiting the T_2 time more than the nuclear-spin dipolar contribution, would be observable for studied concentrations below 100 K even for less purified samples, but also at room temperature depending on the sample and electron-spin-bath concentration.

Very recently a nanophotonic device integrating V2 qubit with excellent spin properties was realized in Ref. [27]. The spin-coherence time is found to be 1.39 ms in a high-purity isotope purified sample. The isotope abundance of the sample is estimated to be $^{28}\text{Si} > 99.85\%$ and $^{12}\text{C} > 99.98\%$. Considering only magnetic field fluctuations due to the residual nuclear-spin bath (approximately 0.15% ^{29}Si), we would expect a coherence time close to 25 ms. The order of magnitude difference indicates that the coherence time is limited by an effect other than nuclear-spin flip flops. Based on our results, interaction with electron spins in the lattice is a possible source of decoherence in this experiment.

Our qualitative and quantitative results are obtained for the quartet silicon vacancy in SiC, with the inhomogenous hyperfine splitting as the main source of degeneracy lifting. The spin Hamiltonian and the results in Fig. 4 can be generalized to other spin-1/2 or spin-3/2 electron-spin-qubit systems not experiencing any additionally major degeneracy splitting. For instance, spin qubits in silicon quantum dots is an area where our findings can be easily generalized and applied [53,54]. Furthermore, our results can be generalized to spin-1 point defect qubits interacting with other spin-1 environmental defects, which can also exhibit nearly degenerate spin states coupled by the dipolar interaction. Although, for spin-1 defects, the differences of the ZFS can also contribute to the splitting of the coupled states and possibly suppress cross-relaxation effects. Relaxation of the spin states is the most efficient when nearby spin-1 defects of the same kind are coupled to each other, e.g., in a dense N- V center ensemble.

ACKNOWLEDGMENTS

We acknowledge support from the Knut and Alice Wallenberg Foundation through WBSQD2 project (Grant No. 2018.0071). Support from the Swedish Government Strategic Research Area SeRC and the Swedish Government Strategic Research Area in Materials Science on Functional Materials at Linköping University (Faculty Grant SFO-Mat-LiU No. 2009 00971) is gratefully acknowledged. This research is supported by the National Research, Development, and Innovation Office of Hungary within the Quantum Information National Laboratory of Hungary (Grant No. 2022-2.1.1-NL-2022-00004) and within the grant FK 145395. N.T.S. acknowledges the support from the EU H2020 project QuanTELCO (Grant No. 862721). The calculations were performed on resources provided by the Swedish National Infrastructure for Computing (SNIC) at the National Supercomputer Centre (NSC), partially funded by the Swedish Research Council through grant agreement no. 2018-05973.

APPENDIX A: CLUSTER-CORRELATION EXPANSION

The cluster-correlation expansion (CCE) is a method for evaluating the coherence function of an ensemble many-body spin system based on a clustering approximation under the assumption of weak coupling between the spins. As outlined in Refs. [55–57], a Hamiltonian like in Eqs. (1) and (2) may have the resulting coherence function cluster-expanded,

$$\mathcal{L} = \mathcal{L}_0 \left(\prod_{i=1}^N \tilde{\mathcal{L}}_i \right) \left(\prod_{i_1 \neq i_2}^N \tilde{\mathcal{L}}_{i_1, i_2} \right) \cdots = \prod_{c \subset C_N} \tilde{\mathcal{L}}_c, \quad (\text{A1})$$

for an N -spin system, C_N , with every possible subsystem contained in C_N and a phase factor \mathcal{L}_0 . The $\tilde{\mathcal{L}}_i$, $\tilde{\mathcal{L}}_{i_1, i_2}$, and $\tilde{\mathcal{L}}_c$ are the spin-correlation functions for clusters of size one involving spin i , two-body clusters involving spins i_1 and i_2 etc., and for an arbitrary cluster c . The factorization is truncated to order M in practice at sufficient accuracy, denoted as performing the CCE- M approach. If applied to systems of limited interaction order, the spin-correlation functions of many-body clusters can be defined recursively, i.e.,

$$\tilde{\mathcal{L}}_c = \frac{\mathcal{L}_c}{\prod_{c' \subset c} \tilde{\mathcal{L}}_{c'}}, \quad (\text{A2})$$

with the spin-coherence function $\mathcal{L}_c = \text{Tr}(\rho_c(t)S_+)/\text{Tr}(\rho_c(0))$ for the c -cluster density matrix ρ_c . The time-evolved cluster-restricted density matrix is obtained by propagation with appropriate propagator, in this case $U(t) = e^{-iH_c t}$ for free decay where H_c is determined by

dropping all terms in Eqs. (1) and (2) not involving spins in cluster c .

In the case of the generalized CCE (gCCE) [58,59], the cluster-expansion approach is applied to the density-matrix components of the qubit, assuming a correlation function expansion of

$$\rho_{ab} = \tilde{\rho}_{ab}^0 \prod \tilde{\rho}_{ab}^i \prod \tilde{\rho}_{ab}^{i_1, i_2} \dots, \quad (\text{A3})$$

and recursion relation

$$\tilde{\rho}_{ab} = \frac{\langle a | \rho_c | b \rangle}{\prod_{c' \subset c} \tilde{\rho}_{ab}^{c'}}. \quad (\text{A4})$$

Expanding the components themselves allows the evolution to also account for relaxation phenomenon and the implied limitation of the coherence in proximity to level anticrossings.

APPENDIX B: THE EXTENDED LINDBLADIAN METHOD

The extended Lindbladian approach is used to simulate the population dynamics of a many-body spin system. The system is modeled to consist of a central spin in an environment of bath spins with dipolar coupling, which Hamiltonian can be written

$$H_{\text{tot}} = H_{\text{defect}} + \sum_{i=1}^{N-1} H_{\text{bath},i} + \sum_{i \neq j}^N H_{i,j}, \quad (\text{B1})$$

corresponding to Eqs. (1) and (2) in this work, with terms, respectively, describing the Hamiltonian of the defect spin labeled as spin 0, the bath spins labeled 1 to $N-1$ and the dipolar interaction terms $H_{i,j}$ between spins i and j . This system is divided into M -body clusters $\{c_k\}$ each containing the defect and $(M-1)$ -bath spins, with respective cluster Hamiltonian

$$H_{c_k} = H_{\text{defect}} + \sum_{i \neq 0, i \in c_k} H_{\text{bath},i} + \sum_{i \neq j; i, j \in c_k} H_{i,j} + \beta_{c_k}, \quad (\text{B2})$$

where β_{c_k} is an effective field to include the spin level change from spins outside the cluster. The time propagation of the system is performed by evolving each cluster density matrix ρ_{c_k} separately while introducing a collective coupling in the form of the extended Lindbladian, \mathcal{L}_{c_k} ,

$$\frac{d\rho_{c_k}}{dt} = -\frac{i}{\hbar} [H_{c_k}, \rho_{c_k}] + \mathcal{L}_{c_k}(\{b_{c_k, mn}\}, \rho_{c_k}). \quad (\text{B3})$$

The Lindbladian coupling for each cluster incorporates the relaxation rate of the defect experienced in other cluster systems due to the bath spins in those clusters and is

defined as

$$\begin{aligned} \mathcal{L}_{c_k}(\{b_{c_k, mn}\}, \rho_{c_k}) &= \sum_{mn} \frac{b_{c_k, mn}}{\text{Tr}(C_{mn}^\dagger C_{mn} \rho_{c_k})} \\ &\times \left(C_{mn} \rho_{c_k} C_{mn}^\dagger - \frac{1}{2} \{ \rho_{c_k}, C_{mn}^\dagger C_{mn} \} \right), \end{aligned} \quad (\text{B4})$$

using the jump operator acting on the defect spin states $|m\rangle$ and $|n\rangle$, $C_{mn} = |m\rangle\langle n| \otimes_{i \in c_k} I_i$, and where the corresponding *dynamic* flip-flop rates $b_{c_k, mn}$ are chosen at the simulation step to achieve the desired description.

The time evolution with the Hamiltonian of Eq. (B2) for a short period time, dt , yields a finite difference that we write as

$$\delta\rho_{c_k} = -\frac{i}{\hbar} [H_{c_k}, \rho_{c_k}(t)] dt. \quad (\text{B5})$$

The defect is also evolved in isolation to give $\delta\rho_d$ as a reference for the inherent effect of the defect Hamiltonian. Using these finite differences, Lindbladian couplings representative of each cluster evolution $a_{c_k, mn}$, as well as for the isolated defect evolution $a_{d, mn}$ are determined and collected to form the collective flip-flop rates

$$b_{c_k, mn} = \sum_{j \neq k} (a_{c_j, mn} - a_{d, mn}), \quad (\text{B6})$$

by having the $a_{c_k, mn}$ couplings satisfy

$$\text{diag}(\text{Tr}_B \delta\rho_{c_k}) = \text{diag}(\text{Tr}_B \mathcal{L}(\{a_{c_k, mn}\}, \rho_{c_k})), \quad (\text{B7})$$

where Tr_B denotes the partial trace over cluster bath spins. Finally, the density matrix populations of each cluster are updated with both the inherent evolution and collective Lindbladian couplings

$$\rho_{c_k}(t + dt) = \rho_{c_k}(t) + \delta\rho_{c_k} + \mathcal{L}(\{b_{c_k, mn}\}, \rho_{c_k}). \quad (\text{B8})$$

We note that the applied method, in principle, allows for an arbitrary cluster size and therefore can be made increasingly precise as necessary. However, for the present work, a two-body clustering of the defect and bath is deemed sufficient.

APPENDIX C: THE EFFECT OF NUCLEAR-SPIN ABUNDANCE ON RELAXATION AND DECOHERENCE

For further description of obtained relaxation and coherence times for the silicon vacancy, shown in Fig. 4 of the paper, we show individual calculation results separately here in Fig. 5. Results are obtained as a function of the ^{29}Si abundance in the local spin environment, although the

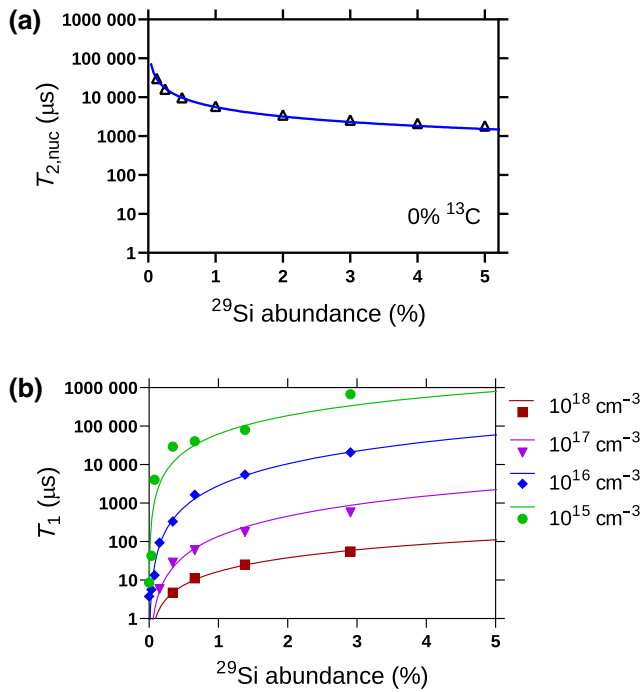


FIG. 5. Data corresponding to Fig. 4, with each individual result shown separately. (a) The coherence time limited by nuclear ^{29}Si spins, as calculated by gCCE-2. (b) The relaxation time for different electron-spin concentrations calculated by the extended Lindbladian method as a function of nuclear-spin abundance determining the inhomogeneous hyperfine splitting field.

abundance for relaxation time calculations corresponded to a hyperfine field splitting described by the inset of Fig. 3. Both kinds of coherence loss could, respectively, be well described by a power law as a function of abundance. In the summary presented in Fig. 4, the limitation, which the relaxation time puts on the coherence time, is taken as $2T_1$, i.e., twice the values presented in Fig. 5(b). Comparing Fig. 5(a) and 5(b), the limit set by the relaxation time is seen to dominate at low abundances, especially for higher electron-spin concentrations.

[1] G. Balasubramanian, P. Neumann, D. Twitchen, M. Markham, R. Kolesov, N. Mizuochi, J. Isoya, J. Achard, J. Beck, J. Tissler, V. Jacques, P. R. Hemmer, F. Jelezko, and J. Wrachtrup, Ultralong spin coherence time in isotopically engineered diamond, *Nat. Mater.* **8**, 383 (2009).
 [2] D. J. Christle, A. L. Falk, P. Andrich, P. V. Klimov, J. U. Hassan, N. T. Son, E. Jánzén, T. Ohshima, and D. D. Awschalom, Isolated electron spins in silicon carbide with millisecond coherence times, *Nat. Mater.* **14**, 160 (2015).
 [3] D. Simin, H. Kraus, A. Sperlich, T. Ohshima, G. V. Astakhov, and V. Dyakonov, Locking of electron spin coherence above 20 ms in natural silicon carbide, *Phys. Rev. B* **95**, 161201(R) (2017).

[4] J. R. Weber, W. F. Koehl, J. B. Varley, A. Janotti, B. B. Buckley, C. G. Van de Walle, and D. D. Awschalom, Quantum computing with defects, *PNAS* **107**, 8513 (2010).
 [5] C. L. Degen, F. Reinhard, and P. Cappellaro, Quantum sensing, *Rev. Mod. Phys.* **89**, 035002 (2017).
 [6] D. D. Awschalom, R. Hanson, J. Wrachtrup, and B. B. Zhou, Quantum technologies with optically interfaced solid-state spins, *Nat. Photonics* **12**, 516 (2018).
 [7] L. Childress, M. V. Gurudev Dutt, J. M. Taylor, A. S. Zibrov, F. Jelezko, J. Wrachtrup, P. R. Hemmer, and M. D. Lukin, Coherent dynamics of coupled electron and nuclear spin qubits in diamond, *Science* **314**, 281 (2006).
 [8] N. Mizuochi, P. Neumann, F. Rempp, J. Beck, V. Jacques, P. Siyushev, K. Nakamura, D. J. Twitchen, H. Watanabe, S. Yamasaki, F. Jelezko, and J. Wrachtrup, Coherence of single spins coupled to a nuclear spin bath of varying density, *Phys. Rev. B* **80**, 041201(R) (2009).
 [9] N. Bar-Gill, L. M. Pham, A. Jarmola, D. Budker, and R. L. Walsworth, Solid-state electronic spin coherence time approaching one second, *Nat. Commun.* **4**, 1743 (2013).
 [10] T. Yamamoto, T. Umeda, K. Watanabe, S. Onoda, M. L. Markham, D. J. Twitchen, B. Naydenov, L. P. McGuinness, T. Teraji, S. Koizumi, F. Dolde, H. Fedder, J. Honert, J. Wrachtrup, T. Ohshima, F. Jelezko, and J. Isoya, Extending spin coherence times of diamond qubits by high-temperature annealing, *Phys. Rev. B* **88**, 075206 (2013).
 [11] E. D. Herbschleb, H. Kato, Y. Maruyama, T. Danjo, T. Makino, S. Yamasaki, I. Ohki, K. Hayashi, H. Morishita, M. Fujiwara, and N. Mizuochi, Ultra-long coherence times amongst room-temperature solid-state spins, *Nat. Commun.* **10**, 3766 (2019).
 [12] C. P. Anderson, E. O. Glen, C. Zeledon, A. Bourassa, Y. Jin, Y. Zhu, C. Vorwerk, A. L. Crook, H. Abe, J. Ul-Hassan, T. Ohshima, N. T. Son, G. Galli, and D. D. Awschalom, Five-second coherence of a single spin with single-shot readout in silicon carbide, *Sci. Adv.* **8**, eabm5912 (2022).
 [13] M. Widmann, S.-Y. Lee, T. Rendler, N. T. Son, H. Fedder, S. Paik, L.-P. Yang, N. Zhao, S. Yang, I. Booker, A. Denisenko, M. Jamali, S. A. Momenzadeh, I. Gerhardt, T. Ohshima, A. Gali, E. Jánzén, and J. Wrachtrup, Coherent control of single spins in silicon carbide at room temperature, *Nat. Mater.* **14**, 164 (2015).
 [14] H. Kraus, V. A. Soltamov, F. Fuchs, D. Simin, A. Sperlich, P. G. Baranov, G. V. Astakhov, and V. Dyakonov, Magnetic field and temperature sensing with atomic-scale spin defects in silicon carbide, *Sci. Rep.* **4**, 5303 (2014).
 [15] S.-Y. Lee, M. Niethammer, and J. Wrachtrup, Vector magnetometry based on $s = \frac{3}{2}$ electronic spins, *Phys. Rev. B* **92**, 115201 (2015).
 [16] D. Simin, V. A. Soltamov, A. V. Poshakinskiy, A. N. Anisimov, R. A. Babunts, D. O. Tolmachev, E. N. Mokhov, M. Trupke, S. A. Tarasenko, A. Sperlich, P. G. Baranov, V. Dyakonov, and G. V. Astakhov, All-optical dc nanoscale magnetometry using silicon vacancy fine structure in isotopically purified silicon carbide, *Phys. Rev. X* **6**, 031014 (2016).
 [17] M. Niethammer, M. Widmann, S.-Y. Lee, P. Stenberg, O. Kordina, T. Ohshima, N. T. Son, E. Jánzén, and J. Wrachtrup, Vector Magnetometry using Silicon Vacancies in 4h-SiC under Ambient Conditions, *Phys. Rev. Appl.* **6**, 034001 (2016).

- [18] A. N. Anisimov, D. Simin, V. A. Soltamov, S. P. Lebedev, P. G. Baranov, G. V. Astakhov, and V. Dyakonov, Optical thermometry based on level anticrossing in silicon carbide, *Sci. Rep.* **6**, 33301 (2016).
- [19] V. A. Soltamov, C. Kasper, A. V. Poshakinskiy, A. N. Anisimov, E. N. Mokhov, A. Sperlich, S. A. Tarasenko, P. G. Baranov, G. V. Astakhov, and V. Dyakonov, Excitation and coherent control of spin qubit modes in silicon carbide at room temperature, *Nat. Commun.* **10**, 1678 (2019).
- [20] T. M. Hoang, H. Ishiwata, Y. Masuyama, Y. Yamazaki, K. Kojima, S.-Y. Lee, T. Ohshima, T. Iwasaki, D. Hisamoto, and M. Hatano, Thermometric quantum sensor using excited state of silicon vacancy centers in $4H$ -SiC devices, *Appl. Phys. Lett.* **118**, 044001 (2021).
- [21] J. B. S. Abraham, C. Gutzsell, D. Todorovski, S. Sperling, J. E. Epstein, B. S. Tien-Street, T. M. Sweeney, J. J. Wathen, E. A. Pogue, P. G. Brereton, T. M. McQueen, W. Frey, B. D. Clader, and R. Osiander, Nanoscale Magnetometry with the Silicon Vacancy in Silicon Carbide, *Phys. Rev. Appl.* **15**, 064022 (2021).
- [22] H. Kraus, V. A. Soltamov, D. Riedel, S. V ath, F. Fuchs, A. Sperlich, P. G. Baranov, V. Dyakonov, and G. V. Astakhov, Room-temperature quantum microwave emitters based on spin defects in silicon carbide, *Nat. Phys.* **10**, 157 (2014).
- [23] P. Udvarhelyi, G. M. H. Thiering, N. Morioka, C. Babin, F. Kaiser, D. Lukin, T. Ohshima, J. Ul-Hassan, N. T. Son, J. Vučkovi c, J. Wrachtrup, and A. Gali, Vibronic States and Their Effect on the Temperature and Strain Dependence of Silicon-Vacancy Qubits in $4H$ -SiC, *Phys. Rev. Appl.* **13**, 054017 (2020).
- [24] P. Udvarhelyi, R. Nagy, F. Kaiser, S.-Y. Lee, J. Wrachtrup, and A. Gali, Spectrally Stable Defect Qubits with No Inversion Symmetry for Robust Spin-to-Photon Interface, *Phys. Rev. Appl.* **11**, 044022 (2019).
- [25] M. Widmann, M. Niethammer, D. Y. Fedyanin, I. A. Khramtsov, T. Rendler, I. D. Booker, J. Ul Hassan, N. Morioka, Y.-C. Chen, I. G. Ivanov, N. T. Son, T. Ohshima, M. Bockstedte, A. Gali, C. Bonato, S.-Y. Lee, and J. Wrachtrup, Electrical charge state manipulation of single silicon vacancies in a silicon carbide quantum optoelectronic device, *Nano Lett.* **19**, 7173 (2019).
- [26] D. M. Lukin, C. Dory, M. A. Guidry, K. Y. Yang, S. D. Mishra, R. Trivedi, M. Radulaski, S. Sun, D. Vercauteren, G. H. Ahn, and J. Vučkovi c, $4H$ -silicon-carbide-on-insulator for integrated quantum and nonlinear photonics, *Nat. Photonics* **14**, 330 (2020).
- [27] C. Babin, *et al.*, Fabrication and nanophotonic waveguide integration of silicon carbide colour centres with preserved spin-optical coherence, *Nat. Mater.* **21**, 67 (2022).
- [28] P. Baranov, I. Il'in, E. Mokhov, M. Muzafarova, S. Orlinskiy, and J. Schmidt, Epr identification of the triplet ground state and photoinduced population inversion for a Si-C divacancy in silicon carbide, *JETP Lett.* **82**, 441 (2005).
- [29] D. Riedel, F. Fuchs, H. Kraus, S. V ath, A. Sperlich, V. Dyakonov, A. A. Soltamova, P. G. Baranov, V. A. Ilyin, and G. V. Astakhov, Resonant Addressing and Manipulation of Silicon Vacancy Qubits in Silicon Carbide, *Phys. Rev. Lett.* **109**, 226402 (2012).
- [30] R. Nagy, M. Niethammer, M. Widmann, Y.-C. Chen, P. Udvarhelyi, C. Bonato, J. U. Hassan, R. Karhu, I. G. Ivanov, N. T. Son, J. R. Maze, T. Ohshima, O. O. Soykal, A. Gali, S.-Y. Lee, F. Kaiser, and J. Wrachtrup, High-fidelity spin and optical control of single silicon-vacancy centres in silicon carbide, *Nat. Commun.* **10**, 1954 (2019).
- [31] N. Morioka, *et al.*, Spin-controlled generation of indistinguishable and distinguishable photons from silicon vacancy centres in silicon carbide, *Nat. Commun.* **11**, 2516 (2020).
- [32] J.-F. Wang, F.-F. Yan, Q. Li, Z.-H. Liu, J.-M. Cui, Z.-D. Liu, A. Gali, J.-S. Xu, C.-F. Li, and G.-C. Guo, Robust coherent control of solid-state spin qubits using anti-Stokes excitation, *Nat. Commun.* **12**, 3223 (2021).
- [33] T. Wimbauer, B. K. Meyer, A. Hofstaetter, A. Scharmann, and H. Overhof, Negatively charged Si vacancy in $4H$ SiC: A comparison between theory and experiment, *Phys. Rev. B* **56**, 7384 (1997).
- [34] N. Mizuochi, S. Yamasaki, H. Takizawa, N. Morishita, T. Ohshima, H. Itoh, and J. Isoya, Continuous-wave and pulsed epr study of the negatively charged silicon vacancy with $s = \frac{3}{2}$ and C_{3v} symmetry in n -type $4H$ -SiC, *Phys. Rev. B* **66**, 235202 (2002).
- [35] S. B. Orlinskiy, J. Schmidt, E. N. Mokhov, and P. G. Baranov, Silicon and carbon vacancies in neutron-irradiated SiC: A high-field electron paramagnetic resonance study, *Phys. Rev. B* **67**, 125207 (2003).
- [36] N. Mizuochi, S. Yamasaki, H. Takizawa, N. Morishita, T. Ohshima, H. Itoh, T. Umeda, and J. Isoya, Spin multiplicity and charge state of a silicon vacancy (T_{12a}) in $4H$ -SiC determined by pulsed endor, *Phys. Rev. B* **72**, 235208 (2005).
- [37] N. T. Son, P. Stenberg, V. Jokubavicius, T. Ohshima, J. U. Hassan, and I. G. Ivanov, Ligand hyperfine interactions at silicon vacancies in $4H$ -SiC, *J. Phys.: Condens. Matter* **31**, 195501 (2019).
- [38] V. Iv ady, J. Davidsson, N. T. Son, T. Ohshima, I. A. Abrikosov, and A. Gali, Identification of Si-vacancy related room-temperature qubits in $4H$ silicon carbide, *Phys. Rev. B* **96**, 161114(R) (2017).
- [39] J. Davidsson, V. Iv ady, R. Armiento, T. Ohshima, N. T. Son, A. Gali, and I. A. Abrikosov, Identification of divacancy and silicon vacancy qubits in $6H$ -SiC, *Appl. Phys. Lett.* **114**, 112107 (2019).
- [40] N. T. Son, P. Carlsson, J. ul Hassan, B. Magnusson, and E. Janz en, Defects and carrier compensation in semi-insulating $4H$ -SiC substrates, *Phys. Rev. B* **75**, 155204 (2007).
- [41] V. Iv ady, I. A. Abrikosov, and A. Gali, First principles calculation of spin-related quantities for point defect qubit research, *npj Comput. Mater.* **4**, 76 (2018).
- [42] V. Iv ady, Longitudinal spin relaxation model applied to point-defect qubit systems, *Phys. Rev. B* **101**, 155203 (2020).
- [43] M. Onizhuk, K. C. Miao, J. P. Blanton, H. Ma, C. P. Anderson, A. Bourassa, D. D. Awschalom, and G. Galli, Probing the Coherence of Solid-State Qubits at Avoided Crossings, *PRX Quantum* **2**, 010311 (2021).
- [44] R. Hanson, V. V. Dobrovitski, A. E. Feiguin, O. Gywat, and D. D. Awschalom, Coherent dynamics of a single spin interacting with an adjustable spin bath, *Science* **320**, 352 (2008).
- [45] N. Bar-Gill, L. Pham, C. Belthangady, D. Le Sage, P. Cappellaro, J. Maze, M. Lukin, A. Yacoby, and R. Walsworth,

- Suppression of spin-bath dynamics for improved coherence of multi-spin-qubit systems, *Nat. Commun.* **3**, 858 (2012).
- [46] O. Bulancea-Lindvall, N. T. Son, I. A. Abrikosov, and V. Ivády, Dipolar spin relaxation of divacancy qubits in silicon carbide, *npj Comput. Mater.* **7**, 1 (2021).
- [47] L.-P. Yang, C. Burk, M. Widmann, S.-Y. Lee, J. Wrachtrup, and N. Zhao, Electron spin decoherence in silicon carbide nuclear spin bath, *Phys. Rev. B* **90**, 241203(R) (2014).
- [48] O. Bulancea-Lindvall, M. T. Eiles, N. T. Son, I. A. Abrikosov, and V. Ivády, Low-Field Microwave-Free Magnetometry using the Dipolar Spin Relaxation of Quartet Spin States in Silicon Carbide, *Phys. Rev. Appl.* **19**, 034006 (2023).
- [49] A. J. Ramsay and A. Rossi, Relaxation dynamics of spin- $\frac{3}{2}$ silicon vacancies in 4H-SiC, *Phys. Rev. B* **101**, 165307 (2020).
- [50] H. J. von Bardeleben, S. A. Zargaleh, J. L. Cantin, W. B. Gao, T. Biktagirov, and U. Gerstmann, Transition metal qubits in 4H-silicon carbide: A correlated EPR and DFT study of the spin $S = 1$ vanadium V3+ center, *Phys. Rev. Mater.* **3**, 124605 (2019).
- [51] H. Singh, A. N. Anisimov, S. S. Nagalyuk, E. N. Mokhov, P. G. Baranov, and D. Suter, Experimental characterization of spin- $\frac{3}{2}$ silicon vacancy centers in 6H-SiC, *Phys. Rev. B* **101**, 134110 (2020).
- [52] V. A. Soltamov, B. V. Yavkin, A. N. Anisimov, H. Singh, A. P. Bundakova, G. V. Mamin, S. B. Orlinskii, E. N. Mokhov, D. Suter, and P. G. Baranov, Relaxation processes and high-field coherent spin manipulation in color center ensembles in 6H-SiC, *Phys. Rev. B* **103**, 195201 (2021).
- [53] A. Chatterjee, P. Stevenson, S. De Franceschi, A. Morello, N. P. de Leon, and F. Kuemmeth, Semiconductor qubits in practice, *Nat. Rev. Phys.* **3**, 157 (2021).
- [54] G. Burkard, T. D. Ladd, J. M. Nichol, A. Pan, and J. R. Petta, Semiconductor spin qubits, *ArXiv:2112.08863* (2021).
- [55] W. Yao, R.-B. Liu, and L. J. Sham, Theory of electron spin decoherence by interacting nuclear spins in a quantum dot, *Phys. Rev. B* **74**, 195301 (2006).
- [56] W. Yang and R.-B. Liu, Quantum many-body theory of qubit decoherence in a finite-size spin bath, *Phys. Rev. B* **78**, 085315 (2008).
- [57] S. Kanai, F. J. Heremans, H. Seo, G. Wolfowicz, C. P. Anderson, S. E. Sullivan, M. Onizhuk, G. Galli, D. D. Awschalom, and H. Ohno, Generalized scaling of spin qubit coherence in over 12 000 host materials, *Proc. Natl. Acad. Sci.* **119**, e2121808119 (2022).
- [58] Z.-S. Yang, Y.-X. Wang, M.-J. Tao, W. Yang, M. Zhang, Q. Ai, and F.-G. Deng, Longitudinal relaxation of a nitrogen-vacancy center in a spin bath by generalized cluster-correlation expansion method, *Ann. Phys.* **413**, 168063 (2020).
- [59] M. Onizhuk, K. C. Miao, J. P. Blanton, H. Ma, C. P. Anderson, A. Bourassa, D. D. Awschalom, and G. Galli, Probing the Coherence of Solid-State Qubits at Avoided Crossings, *PRX Quantum* **2**, 010311 (2021).